Artificial Force Induced Reaction (AFIR) Method for Exploring Quantum Chemical Potential Energy Surfaces

Satoshi Maeda,[*,†] Yu Harabuchi,[†] Makito Takagi,[‡] Tetsuya Taketsugu,[†] Keiji Morokuma[§]

[†]Department of Chemistry, Faculty of Science, Hokkaido University, Sapporo 060-0810, Japan.

[‡]Graduate School of Chemical Sciences and Engineering, Hokkaido University, Sapporo 060-8628, Japan

[§]Fukui Institute for Fundamental Chemistry, Kyoto University, Kyoto 606-8103, Japan

Abstract

In this account, a technical overview of the artificial force induced reaction (AFIR) method is presented. The AFIR method is one of automated reaction path search methods developed by the authors, and has been applied extensively to a variety of chemical reactions such as organocatalysis, organometallic catalysis, and photoreactions. There are two modes in the AFIR method, i.e., multi-component mode (MC-AFIR) and

single-component mode (SC-AFIR). The former has been applied to bimolecular and multicomponent reactions and the latter to unimolecular isomerization and dissociation reactions. Five numerical examples are presented for Aldol reaction, Claisen rearrangement, Co-catalyzed hydroformylation, a fullerene structure search, and a non-radiative decay path search in an electronically excited naphthalene molecule. Finally, possible applications of the AFIR method are discussed.

Keywords: potential energy surface, transition state, conical intersection, intrinsic reaction coordinate, artificial force induced reaction (AFIR)

Table of Contents

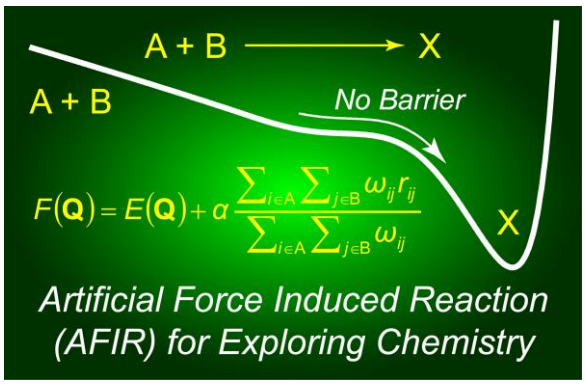

Finding reaction paths: Artificial force induced reaction (AFIR) method has been developed for exploring chemical structures and reaction pathways in computers. A

technical overview of the AFIR method is presented together with some numerical examples. Numerical results demonstrated its high applicability and efficiency.

1. Introduction

Recent advances in quantum chemistry and computer technology enabled application of quantum chemical calculations to various problems in chemistry.[1] In particular, significant contributions have been made in the area of mechanistic study of homogeneous catalysis.[2-7] In these studies, geometries of intermediates (IMs) and transition states (TSs) have been investigated by geometry optimization.[8] In studies of reactions involving electronic excited states, geometries of minima on the seam of crossing between two or more electronic states as well as IMs and TSs on the electronic excited state have been optimized.[9-13] Recently, geometry optimization is made routinely even in systems containing hundred or more atoms, and therefore is a very powerful tool in studies of the mechanism of chemical reactions on the basis of quantum chemical calculations.

However, there is a problem in geometry optimization. Namely, it generally requires a good guess or previous knowledge of the reaction mechanism. Such inputs may be a guess of transition state, knowledge on IMs and/or products, an estimate of

reaction variables, etc. It is therefore difficult to study highly complicated multistep reactions or those for which limited previous knowledge is available. A systematic approach that can explore important geometries automatically needs to be developed.[14-16] Although there have been considerable efforts in development of such automated searching approaches,[17-45] a comprehensive review of various existing methods is beyond the scope of this personal account. This account focus on the artificial force induced reaction[46-49] (AFIR) method, developed by ourselves and implemented in the GRRM (global reaction route mapping) program.[50,51] The AFIR has been applied most extensively to organo and organometallic catalysis in combination with quantum chemical calculations.[52-64] The other applications are to gas-phase reactions,[65-67] enzyme catalysis,[68] domino reaction,[69] and metal cluster catalysis.[70,71] It has also been applied to electronic excited states and geometries of seam of crossing between two electronic states.[72-75] In this account, a technical overview of the AFIR method is provided with some numerical examples.

2. Artificial Force Induced Reaction (AFIR) method

2.1 AFIR function

The idea of AFIR is simple; just push fragments A and B together or pull them apart.

When both A and B are atoms, they can be pushed together by adding a linear function of their distance r_{AB} to their potential energy $E(r_{AB})$. In Fig. 1, a diatomic potential curve $E(r_{AB})$ is shown. This curve has a barrier which separates the reactant pair A + B and the product X. This barrier can be eliminated by adding the term αr_{AB} to $E(r_{AB})$, where α is a constant parameter. The resulting function which is shown in blue in Fig. 1 has no barrier. On this function $E(r_{AB}) + \alpha r_{AB}$, the product region can be reached efficiently from the reactant pair just by minimizing the function.

The same procedure can be done in polyatomic systems by minimizing the following AFIR function:[46-49]

$$F(\mathbf{Q}) = E(\mathbf{Q}) + \rho\alpha \frac{\sum_{i\in A}\sum_{j\in B}\omega_{ij}r_{ij}}{\sum_{i\in A}\sum_{j\in B}\omega_{ij}} \qquad (1)$$

This function consists of two terms, i.e., the Born-Oppenheimer potential energy surface (PES) $E(\mathbf{Q})$ of geometrical parameters $\mathbf{Q}$ and the artificial force term. The parameter α in the artificial force term determines the strength of force. The coefficient ρ is either 1 to push fragments together or −1 to pull them apart. The force term is given as a weighted sum of the distance r_{ij} between atom i in the fragment A and atom j in the fragment B, and the weight function ω_{ij} is:

$$\omega_{ij} = \left[\frac{(R_i + R_j)}{r_{ij}}\right]^p \qquad (2)$$

This weight function puts a stronger force to the closer atom pairs and a weaker force to the more distant pairs. In eq. (2), the inverse distance $1/r_{ij}$ is scaled by $R_i + R_j$, the sum of covalent radii of atoms i and j, to treat all elements equivalently. It was confirmed that results did not strongly depend on the choice of p,[46] and p is usually set to 6.0.

For convenience, the parameter α is determined by the following equation.

$$\alpha = \frac{\gamma}{\left[2^{-\frac{1}{6}} - \left(1+\sqrt{1+\frac{\gamma}{\varepsilon}}\right)^{-\frac{1}{6}}\right] R_0} \qquad (3)$$

This α corresponds to the mean force that acts on two atoms in their direct collision on the Lennard-Jones (LJ) potential with collision energy γ, in the area from the minimum to the turning point. The standard Ar-Ar parameters of the LJ potential, i.e., R_0 = 3.8164 Å and ε = 1.0061 kJ/mol, were employed. The model collision energy parameter γ defines an *approximate* upper limit of the barrier height that can be eliminated by the force term. The γ parameter can be chosen by users, depending approximately on the highest TS energies searched. A choice of γ parameter may also be justified based on experimental conditions such as temperature T, reaction time t, etc. In all examples presented below, the γ value was decided assuming the rate constant k of the standard transition state theory.[76]

$$k = \frac{k_B T}{h} \exp\left[-\frac{\Delta\Delta G^{\ddagger}}{RT} \right] \qquad (4)$$

In eq. (4), $\Delta\Delta G^{\ddagger}$ is the *overall* Gibbs free energy of activation, k_B is the Boltzmann constant, T is the temperature, h is the Planck constant and R is the gas constant. The reaction time t can be estimated as the inverse of the rate constant, i.e., $t \approx 1/k$. By substituting $k = 1/t$ and taking inverse and natural logarithm of the both sides of eq. (4), the γ required to overcome the barrier of $\Delta\Delta G^{\ddagger}$ can be estimated as follows.

$$\gamma = RT\left(\ln t - \ln \frac{h}{k_B T} \right) \qquad (5)$$

Temperature T assumed in each calculation is described in the corresponding section. One should set t to a larger value than those in actual reactions. This is because γ provides just an *approximate* upper limit of the barrier height. It is thus recommended to use a large value not to overlook important paths. Hence, t was set to 10 days in all the examples in this paper. For example, at T = 298.15 K, γ = 93.3 kJ/mol when t = 1 hour, γ = 101.2 kJ/mol when t = 1 day, and γ = 106.9 kJ/mol when t = 10 days. The γ value determined with t = 10 days is larger by ~15% compared to the case t = 1 hour. It should also be noted that a search with a very large γ gives many high barrier pathways that are not important in a given experimental condition, and such an exhaustive search requires very large computational costs.

We note here that adding an artificial force to specified atoms has been previously made for various methods. For example, in the steered molecular dynamics (MD), a force has been added to selected atoms to accelerate an MD toward a specific direction or to simulate mechanochemical dynamics.[77] A force term described by the linear function of atom-atom distance has been added to the PES and the resulting model function has been used for discussing geometrical transformations under a mechanical force introduced by an external stimulus.[78-80] A force was also added for empirical corrections of molecular geometries in geometry optimization.[81] At nearly the same time, two groups independently suggested use of an artificial force in the purpose for obtaining an approximate reaction path and related TSs, where one of them has been termed AFIR[46] and the other enforced geometry optimization[35] (EGO). EGO adds a force between two selected atoms. The way to add a force in AFIR is different from in EGO; AFIR can put a force not only between atoms but also between polyatomic fragments using the AFIR function. This feature allowed for the use of AFIR in automated pathway sampling with the multicomponent algorithm described below. Significance of the use of the AFIR function was discussed previously in more detail.[47] As shown below, AFIR has been further used and established as an efficient automated reaction path search method for a range of practical applications.

2.2 AFIR path

The force term in eq. (1) eliminates barriers along a reaction path, and allows for reaching a product very efficiently just by minimizing the AFIR function. Such a path obtained by minimization of the AFIR function is called AFIR path. The AFIR function includes $E(\mathbf{Q})$, and the AFIR path is expected to pass low energy regions near corresponding TSs. Actually, it was shown that the maximum energy point along the AFIR path was a good guess of the corresponding TS.[46-49] A reaction path can be obtained by optimizing a TS starting from the maximum energy point on the AFIR path and subsequently doing an intrinsic reaction coordinate[82,83] (IRC) path calculation starting from the obtained TS.

This procedure may fail to find shallow TSs. This happens especially when γ is much larger than the barrier in the target reaction. To reduce such cases, relaxation of the AFIR path has been made before optimizing TSs. Although this can be done by any path optimization method,[84-89] in this study the locally updated planes[85] (LUP) method was employed. In the LUP method, path points are evenly distributed along a given path and moved to lower energy points in the hyperplane perpendicular to the path tangent. This procedure, i.e., evenly distributing the path points and relaxing them toward lower

energy points in the hyperplane, is repeated until certain termination criteria are met. In this study, this was repeated 15 times in total, where path points were distributed in every ~1.0 Å in the first 10 cycles and in every ~0.5 Å in the last 5 cycles. The two terminal points were optimized directly to local minima (MINs). At the other point p_i, the path tangent was defined as the tangent to a circle that includes three successive path points p_{i-1}, p_i, and p_{i+1}. Maximum energy points were treated separately, and optimized directly to the highest points.[86] Finally, all maximum energy points and minimum energy points along the path obtained after 15 LUP cycles were optimized to TSs and MINs, respectively, using a standard geometry optimization method described below.

Local optimization, i.e., AFIR function minimization, LUP path optimization, TS optimization, and MIN optimization, were made by combined rational function optimization[90] (RFO) and quadratic approximation[91] (QA) methods. An optimization step was at first determined by the RFO method. The RFO step was adopted when the step size was smaller than a given trust radius (R_T). If the size of RFO step exceeded R_T, then the step was determined by the QA method. The QA method gives an optimization step whose size exactly matches R_T. The R_T value was set to 0.5 Å in AFIR function minimization, in the first 10 cycles of LUP path optimization, and in MIN optimization, while it was set to 0.1 Å in the last 5 cycles of LUP path optimization and in TS

optimization. The search can be done either with or without exact Hessian. In the with-Hessian search, exact Hessian is computed in every m optimization steps and updated. In the default setting of the GRRM program,[50,51] m = 5 in TS optimization and m = 50 in AFIR function minimization, LUP path optimization, and MIN optimization. In the without-Hessian search, the initial Hessian was estimated by a simple force field in which all atom pairs were assumed to be linked by a spring with a force constant $\varepsilon_{ij} = 2.0e^{-1.6\left[r_{ij}/\left(R_i+R_j\right)\right]^2}$ au. Then, this very crude Hessian was updated by Hessian updating methods. In TS optimization and LUP path optimization, Bofill's Hessian updating method combining Powel's equation and the SR1 equation with Bofill's parameter was employed.[92] While, in AFIR function minimization and MIN optimization, Farkas and Schlegel's method combining the BFGS and SR1 equations by the square root of Bofill's parameter was applied.[93] Furthermore, gradient vectors not only at the last step but also at several previous steps were used in Hessian updating.[93]

IRC path calculations were made starting from all obtained TSs. This is generally necessary to discuss which pair of MINs is connected by the TS. This is because such a path connectivity may alter depending on the nature of path. For example, the connectivity may change whether to adopt the mass-weighted coordinate or not in steepest descent path calculations.[16] In this study, IRC calculations were made by the

local quadratic approximation (LQA) method.[94] In the without-Hessian search, the first IRC points in forward and backward IRC path calculations were obtained as minima on the hypersphere centered at the TS. In the quadratic approximation at the TS, these points are located on the imaginary frequency mode. Then, the IRC path was followed by the LQA method using Bofill's Hessian updating method.[92] In the with-Hessian search, exact Hessian was computed in every 10 steps.

The flow of the single AFIR path calculation can be summarized as follows:

1. Minimize the AFIR function for given fragments and γ (the force term is applied only in this step).
2. Relax the AFIR path by the LUP method.
3. Optimize maxima and minima on the relaxed path to TSs and MINs, respectively, by the combined RFO/QA geometry optimization method.
4. Calculate the IRC path by the LQA method starting from all obtained TSs.

An option is available to skip TS optimization and IRC calculation. This option is used to accelerate the search of MINs only. In this case, the flow is simplified as follows:

1. Minimize the AFIR function for given fragments and γ (the force term is applied only in this step).

2. Optimize minima on the AFIR path to MINs by the combined RFO/QA geometry optimization method.

It should be emphasized that all MINs and TSs obtained and discussed below are local minima and first-order saddles, respectively, on the PES without the force term. Furthermore, from all the TSs, IRC calculations were made to confirm the connectivity of IRC paths.

2.3 Multi-component algorithm

The AFIR has originally been developed for bimolecular and multicomponent reactions.[46-48] The algorithm for such reactions has been called multicomponent AFIR (MC-AFIR). In MC-AFIR, fragments A and B in eq. (1) correspond to reactant molecules or a part of them. When the third reactant C exists, two additional terms to apply forces between A and C and between B and C are added. At first, their initial mutual orientations and approach positions are randomly generated. Then, starting from the random structure, the AFIR function is minimized to obtain the corresponding AFIR path. By repeating the random structure generation and AFIR function minimization, one can obtain many AFIR paths automatically. This cycle is stopped if no new product is found in the latest *n* AFIR paths. Finally, LUP path optimization, TS optimization,

and IRC path calculation are applied successively to all obtained AFIR paths, and related MINs, TSs, and IRC paths are identified. These multistep calculations are all automated in the developmental version of GRRM program.[50] In MC-AFIR, these AFIR path calculations can be executed in parallel.

2.4 Single-component algorithm

The AFIR was extended for reactions that occur in a single molecule.[49] The algorithm introduced for this purpose has been termed single-component AFIR (SC-AFIR). In SC-AFIR, fragments A and B in eq. (1) are systematically defined in a single molecule.

At first, two atoms *k* and *l* are chosen. Then, a perturbed structure is generated by the following two steps: (1) the distance of the two atoms is reduced / increased by *x*% (*x* = 20 in the following examples), and (2) positions of the other atoms are optimized by the least squares fitting in which the root mean square error between elements in the distance matrix for the original structure and those for the perturbed structure is minimized. This treatment is important especially when the original structure has a (local) symmetry. For example, in a linear tri-atomic molecule P-Q-R, the positive force applied between P and R will just reduce the length of the molecule and never give a non-linear structure. On the other hand, the perturbed structure determined by this

procedure is non-linear, and the positive force smoothly leads to its triangle-shaped isomer. It should be noted that no quantum chemical calculation is required in generation of the perturbed structure.

In the perturbed structure, fragments A and B are defined around the atoms *k* and *l*. First, *k* and *l* are included in A and B, respectively. Then, all atoms connected to A or B are included in A or B, respectively, where atoms *i* and *j* are regarded to be connected when $r_{ij} / (R_i + R_j) < 1.5$. This selection is done twice, and atoms directly connected to *k* and *l* (first layer) and those connected to them (second layer) are included in A and B, respectively. Finally, atoms *i* in A and *j* in B are excluded from A and B, respectively, when $r_{ij} / (R_i + R_j) < r_{kl} / (R_k + R_l)$.

Once the two fragments A and B are defined in the perturbed structure, the corresponding AFIR function is minimized. As usual, this will give an AFIR path, and the subsequent LUP path optimization, TS optimization, and IRC calculation give related MINs, TSs, and IRC paths. By applying this procedure to all atom pairs except for those with very long distances ($r_{ij} / (R_i + R_j) > 5.0$), reaction paths can be searched systematically starting from the molecule. In the latest implementation, atom pairs that are identical to the other pair when symmetry is considered are excluded. In SC-AFIR, these AFIR path calculations can also be done in parallel.

The above procedure is at first applied to the initial MIN. The initial MIN can either be prepared by users or be generated randomly. Then, some new MINs that are connected to the initial MIN with an IRC path will be obtained. There are several options to control the further search. If only paths connected to the initial MIN are subjects of interest, the further search is not considered. By applying the SC-AFIR to all obtained MINs one after another, a global (or semi-global) PES area accessible with the given γ can be mapped out. The search can be confined to low energy regions or PES areas including structures having a specified bond-connectivity, by omitting applications of the SC-AFIR to MINs with high energy or those without specified bond-connectivity. These confined searches are much more efficient than the global search.

In such confined searches, those far from the initial MIN will not be considered. A simple stochastic algorithm is available to reach low energy MINs in different regions of the PES efficiently.[71] In this algorithm, the following parameter μ_i is computed for all MINs in selecting a MIN to which the SC-AFIR is applied.

$$\mu_i = \xi_i \frac{\exp\left[-\Delta G_i / RT_{\mathrm{R}}\right]}{\sum_j^{\mathrm{all\,MINs}} \exp\left[-\Delta G_j / RT_{\mathrm{R}}\right]} \qquad (6)$$

Then, a MIN that has the maximum μ value is chosen. In the expression of μ_i, ξ_i is a random number between 0 and 1 and ΔG_i is Gibbs free energy of MIN i. The T_{R} is a model temperature parameter, which determines how frequently high energy MINs are

chosen and is usually set to a much higher value than the corresponding experimental temperature. In the without-Hessian search, electronic energy ΔE_i is adopted instead of ΔG_i because ΔG_i is available only when exact Hessian is computed. In addition, distant atom pairs that are omitted in the usual SC-AFIR procedure are considered sometimes (once in N AFIR path calculations in an N atom system) to induce a large structural deformation. The search is terminated when the latest P AFIR paths do not update the lowest Q minima. In the previous study, Q and P were set to N and $3N$, respectively, in systems including N atoms.[71]

2.5 Multi-state calculation

Automated reaction path search methods can be applied to reactions involving multiple electronic states using two model function approaches. These approaches were introduced in combination with the other automated reaction path search method,[34,36] and described in a recent review together with some examples on small systems.[13,40]

In exploration of structures of the minimum energy seam of crossing (MESX) or the minimum energy conical intersection (MECI) between two states, one can apply the seam model function (SMF) approach.[34] MESX is a minimum energy point within the seam of crossing hypersurface ($f-1$ dimensional, where f is the internal degrees of

freedom) between two states with different spin or spatial symmetry, and MECI is a minimum energy point within the conical intersection hypersurface ($f-2$ dimensional) between two states with the same spin and spatial symmetry. In the SMF approach, MINs on the following model function are explored.

$$F^{\mathrm{SMF}}(\mathbf{Q}) = \frac{1}{2}\left[E^{\mathrm{State\text{-}1}}(\mathbf{Q}) + E^{\mathrm{State\text{-}2}}(\mathbf{Q})\right] + \frac{\left[E^{\mathrm{State\text{-}1}}(\mathbf{Q}) - E^{\mathrm{State\text{-}2}}(\mathbf{Q})\right]^2}{\beta} \qquad (7)$$

In eq. (7), $E^{\mathrm{State\text{-}1}}(\mathbf{Q})$ and $E^{\mathrm{State\text{-}2}}(\mathbf{Q})$ are adiabatic PESs for the two target electronic states, and β is a constant parameter (set to 30 kJ/mol in this and previous studies). MINs on $F^{\mathrm{SMF}}(\mathbf{Q})$ are located near corresponding MESXs or MECIs. Therefore, MINs on $F^{\mathrm{SMF}}(\mathbf{Q})$ are explored by the AFIR method at first.[72,73] Specifically, $F^{\mathrm{SMF}}(\mathbf{Q})$ is substituted to $E(\mathbf{Q})$ in eq. (1), and the AFIR function consisting of $F^{\mathrm{SMF}}(\mathbf{Q})$ and the force term is minimized to reach different MINs on $F^{\mathrm{SMF}}(\mathbf{Q})$. Then, all obtained MINs on $F^{\mathrm{SMF}}(\mathbf{Q})$ are reoptimized by any standard MESX / MECI optimization method. In this study, the gradient projection[95] (GP) method combined with the branching plane update[96] (BPU) approach was employed.

On PESs of electronic excited states, there are many singular points in low energy regions due to conical intersections with the lower state. To avoid this problem, the avoiding model function (AMF) approach was introduced.[36] In AMF, MINs and TSs on the following model function are explored.

$$F^{\mathrm{AMF}}(\mathbf{Q}) = \frac{1}{2}\left(E^{\text{State-1}}(\mathbf{Q}) + E^{\text{State-2}}(\mathbf{Q})\right) + \frac{1}{2}\sqrt{\left(E^{\text{State-1}}(\mathbf{Q}) - E^{\text{State-2}}(\mathbf{Q})\right)^2 + 4U^2}$$
$$U(\mathbf{Q}) = \frac{\chi}{2}\exp\left[-\left(\frac{E^{\text{state-1}}(\mathbf{Q}) - E^{\text{state-2}}(\mathbf{Q})}{\chi}\right)^2\right] \quad (8)$$

In $F^{\mathrm{AMF}}(\mathbf{Q})$, $E^{\text{State-1}}(\mathbf{Q})$ is an adiabatic PES of the upper (target) state, $E^{\text{State-2}}(\mathbf{Q})$ is an adiabatic PES of the lower state, and χ is a constant parameter (set to 30 kJ/mol in previous studies). In TS regions, $F^{\mathrm{AMF}}(\mathbf{Q})$ is nearly identical to $E^{\text{State-1}}(\mathbf{Q})$. On the other hand, in conical intersection regions between the two states, $F^{\mathrm{AMF}}(\mathbf{Q})$ has a smooth, avoided-crossing-like shape, in contrast to singular $E^{\text{State-1}}(\mathbf{Q})$. This allows for exploration of excited state TSs by any automated reaction path search method. When it is combined with AFIR, $F^{\mathrm{AMF}}(\mathbf{Q})$ is substituted to $E(\mathbf{Q})$ in eq. (1), and AFIR paths on $F^{\mathrm{AMF}}(\mathbf{Q})$ are explored.[72] TSs and MINs on $F^{\mathrm{AMF}}(\mathbf{Q})$ are *approximate* structures. All these structures are finally reoptimized on $E^{\text{State-1}}(\mathbf{Q})$ by any standard geometry optimization technique.

3. Results

3.1 Aldol reaction

Aldol reaction is one of the simplest bimolecular reactions.[97] Performance of the MC-AFIR method implemented in the latest developmental version of GRRM was examined using the simplest substrate pair, i.e., formaldehyde and vinyl alcohol. In this

application, three structures were read in. These three correspond to structures of formaldehyde, cis-isomer of vinyl alcohol, and its trans-isomer. In our previous study, only the former two were used;[47] the search corresponded to a conformation specific search. In this calculation, the MC-AFIR cycle was terminated when no new product was obtained in the latest 100 AFIR paths. The parameter γ in eq. (3) was set to 106.9 kJ/mol, i.e., T = 298.15 K and t = 10 days in eq. (5). Both with-Hessian and without-Hessian calculations were tested. Since the search is stochastic, identical calculation was performed 10 times with different random number seeds to see the statistics. The searches were done at the spin-restricted B3LYP/6-31G level.

With this γ, only one path was found. This single path, which is shown at the left top in Fig. 2, corresponds to the path of Aldol reaction. This path was found in all the 20 calculations, i.e., 10 with-Hessian calculations and 10 without-Hessian calculations. The average numbers of gradient and Hessian calculations required to complete the search were 6716 and 233, respectively, in the with-Hessian calculations. On the other hand, the average number of gradient calculations required in the without-Hessian calculations were 6898. It should be noted that these numbers are the sum of all calculations including TS optimizations and IRC path calculations. The average numbers of gradient and Hessian calculations that were done before the first detection of the Aldol product

were 1015 and 29, respectively, in the with-Hessian calculations. The average number of gradient calculations that were made before the first detection of the Aldol product was 602 in the without-Hessian calculations.

In addition, an unrealistic calculation was performed to see what happened when unreasonably large γ was adopted. In this calculation, the initial γ was randomly given between 106.9 and 1069 kJ/mol in each AFIR path calculation, and the γ value was gradually increased up to 1069 kJ/mol. The with-Hessian algorithm was applied. The other settings were the same to those adopted in the above calculations. All obtained paths that possess a TS are listed in Fig. 2 in ascending order in terms of relative Gibbs free energy value of TS, where relative electronic energy values are also shown in parentheses. These energy values are relative to the sum of energies of separately optimized formaldehyde and the cis-isomer of vinyl alcohol. In addition to these paths, many high energy pathways that do not have any TS and generate radical pairs such as HCO + CH_3-CH-OH were found. Obviously, these radical channels as well as paths in Fig. 2 except for the Aldol one are unimportant in mechanistic studies of Aldol reactions. The numbers of gradient and Hessian calculations required to complete the whole calculation including TS optimizations and IRC path calculations were 270287 and 11919, respectively. This result emphasizes importance of the choice of the γ value to

enhance efficiency. Use of eq. (5) suggested in this paper was reasonable.

3.2 Claisen rearrangement

Claisen rearrangement of an allyl vinyl ether is a fundamental unimolecular reaction.[97] Performance of the SC-AFIR method was tested with this reaction using the simplest substrate CH_2=CH-O-CH_2-CH=CH_2. This reaction was experimentally performed at high temperatures ~470.15 K;[98] therefore a relatively large γ = 171.5 kJ/mol (T = 470.15 K, t = 10 days) was adopted. In this calculation, the SC-AFIR search was applied to MINs that had the bond connectivity corresponding to CH_2=CH-O-CH_2-CH=CH_2. Namely, IRC paths connected to one of conformers of CH_2=CH-O-CH_2-CH=CH_2 were explored. Furthermore, both with-Hessian and without-Hessian calculations were performed for comparison. These searches were done at the spin-restricted B3LYP/6-31G level.

All obtained MINs and TSs in the two calculations are listed in Fig. 3. In the labels of structures, both relative Gibbs free energy and electronic energy in parentheses are shown. TS*x*/*y* is a TS along the IRC path connecting MIN*x* and MIN*y*. There are two bond rearranging TSs, i.e., TS2/11 and TS6/15, in this list, and these two correspond to the chair- and boat-type TSs, respectively, of Claisen rearrangement.[99] All the other TSs

except for TS12/13 and TS12/15 are for conformational rearrangements between conformers of allyl vinyl ether. Importance of the conformational rearrangement path network in accurate prediction of experimental rate constants[100] and also in discussions of time scale hierarchy in reaction networks[101] were discussed very recently. The SC-AFIR search successfully identified both kinetically slow chemical bond reorganization paths and fast conformational rearrangement paths in a single theoretical framework. No kinetically unimportant product was found in the search with γ = 171.5, and this also justified the use of eq. (5) in deciding the γ value.

Structures missed in the without-Hessian calculation are indicated by * in the structure labels in Fig. 3. The with- and without-Hessian calculations gave essentially an identical result. All pathways connected to MINs that have the bond connectivity corresponding to CH_2=CH-O-CH_2-CH=CH_2 obtained by the with-Hessian calculation were found also by the without-Hessian calculation. Only differences are seen in the product region. This difference arose by subtle differences in AFIR paths going over the high TS12/13 and TS12/15. It is known that paths may reach different MINs depending on subtle differences in path nature when the MINs are connected by a barrier that is much lower than the highest point of the path.[16] This happened in AFIR paths computed by different integration algorithms. However, this was not a problem in this application.

This is because paths connecting conformers in the product region were not the subject of the search as specified in the computational setup. In the with-Hessian calculation, 68169 and 8954 times gradient and Hessian calculations were made in total. In the without-Hessian calculation, 104832 times gradient calculations were done in whole including TS optimizations and IRC path calculations. The subtle increase in the number of gradient calculations in the without-Hessian calculation is due to the slower convergence in geometry optimizations. We note that in the without-Hessian calculation, Gibbs free energy is not available because Hessian is required to compute vibrational free energy corrections.

3.3 Co-catalyzed hydroformylation

In the next example, MC- and SC-AFIR were combined. Hydrogen H_2, carbon monoxide CO, and ethylene C_2H_4 are reactants and cobalt hydride carbonyl complex $HCo(CO)_3$ is a catalyst. This reaction known as hydroformylation affords propionaldehyde C_2H_5CHO.[102] Its mechanism and kinetics have been studied both experimentally and theoretically.[103-108] In the following calculations, it was assumed that only one H_2, one CO, one C_2H_4, and one $HCo(CO)_3$ were involved. In MC-AFIR calculations, some atoms, O atom in CO, H atoms in C_2H_4, and all atoms except for Co

in $HCo(CO)_3$, were excluded from A and B in eq. (1). In SC-AFIR calculations, the perturbed structure generation, fragments definition, and resulting AFIR function minimization were not applied to atom pairs including one of the following atoms: O atom in CO, H atoms in C_2H_4, and O atoms in $HCo(CO)_3$. Based on a typical experimental temperature, γ was set to 153.0 kJ/mol (T = 403.15 K, t = 10 days). The search was done at the spin-restricted B3LYP/6-31G level using the with-Hessian algorithm.

Obtained structures are listed in Figs 4-6. In these figures, important structures that are used in further growth of the structural list are indicated by *. DC stands for dissociation channel, and corresponding DCs are described in captions. To obtain these structures, several MC- and SC-AFIR calculations were done sequentially. At first, MC-AFIR was applied to the $H_2/HCo(CO)_3$, $CO/HCo(CO)_3$, and $C_2H_4/HCo(CO)_3$ pairs. These three calculations gave MIN5, MIN6, and MIN7 in Fig. 4, and required 767 gradient and 32 Hessian in $H_2/HCo(CO)_3$, 1242 and 125 in $CO/HCo(CO)_3$, and 1180 and 82 in $C_2H_4/HCo(CO)_3$. All these paths were barrierless, and their kinetic importance was equivalent. Thermodynamically, MIN6 was the most preferable. Therefore, MC-AFIR was applied further to the H_2/MIN6 and C_2H_4/MIN6 pairs. These calculations, that required 584 gradient and 44 Hessian in H_2/MIN6 and 409 and 13 in

C_2H_4/MIN6, gave no additional structure with the present γ. An application of SC-AFIR to MIN6, which required 558 gradient and 75 Hessian, resulted in a path of pseudo rotation through TS6/6. Then, MIN7 was chosen as the second most preferable intermediate. An application of MC-AFIR to the H_2/MIN7 pair, which required 610 gradient and 25 Hessian, did not give any new structure. An application of MC-AFIR to the CO/MIN7 pair, which required 17422 gradient and 1570 Hessian, generated several high barrier paths for ligand exchanges. On the other hand, an application of SC-AFIR to MIN7, which required 6435 gradient and 874 Hessian, gave a kinetically preferable intermediate MIN10. An application of SC-AFIR to MIN10, which required 2143 gradient and 306 Hessian, confirmed that MIN10 is also preferable thermodynamically among its isomers; MIN10 was chosen for the next step.

Applications of MC-AFIR to the H_2/MIN10 and CO/MIN10 pairs, that required 1813 gradient and 139 Hessian in H_2/MIN10 and 3017 and 315 in CO/MIN10, gave MIN18 in Fig. 5 as a kinetically preferable intermediate. Then, an SC-AFIR calculation starting from MIN18, which required 3928 gradient and 512 Hessian, found MIN19 as a kinetically preferable intermediate. An application of SC-AFIR to MIN19, which required 16428 gradient and 2027 Hessian, found MIN20 and confirmed that MIN20 was preferable both kinetically and thermodynamically. An application of MC-AFIR to

the H_2/MIN20 pair, which required 2133 gradient and 186 Hessian, gave MIN24 as a kinetically preferable intermediate. Finally, an SC-AFIR calculation starting from MIN24, which required 168124 gradient and 22180 Hessian, gave complexes between $HCo(CO)_3$ and C_2H_5CHO. At this stage, the original catalyst was reproduced and the product of hydroformylation was obtained. Therefore, a fully-systematic prediction of the full-catalytic cycle was completed at this stage.

The structural list in Figs. 4-6 is much more perfected than the list published previously by ourselves.[53] On the other hand, computational costs also increased substantially. This is because SC-AFIR was used in this study in the isomerization stages. Previously, each ligand was used as fragments A and B in eq. (1).[53] For example, whole of the -CO-CH_2-CH_3 part was considered to be one fragment. This treatment was not enough to find all isomerization TSs shown in Figs. 4-6. Previously, only one H-atom transfer TS, i.e., TS29/DC11, was found for the final step.[53] In this study, six such TSs were found. In an accurate prediction of reaction barrier and selectivity, finding all low-lying TSs is necessary for each elementary step. We also note that for the final step 94 MINs and 158 TSs were located in total. Among them, only MINs having the bond connectivity of MIN24 are shown in Figs 5 and 6 for clarity. Concerning TSs, those connecting a pair of two MINs among MIN24-41 and those connecting one of

these MINs and a DC are presented. In the 94 MINs, a structure having an OH moiety is included, and this is considered to be a precursor of an alcohol byproduct. In Figs. 4-6, there are many other paths leading to resting states and/or byproducts. Such paths are not directly involved in the catalytic cycle, but must be considered to discuss kinetics and selectivity. The present calculation with γ = 153.0 kJ/mol (T = 403.15 K, t = 10 days in eq. (5)) gave a reasonable set structures to understand not only mechanism but also kinetics and selectivity.

3.4 Fullerene from scratch

As a case study of the stochastic SC-AFIR algorithm, a search for the structure of Buckminsterfullerene was performed. In this example, TSs were not optimized. Namely, LUP optimization, TS optimization, and IRC path calculation were skipped during the search, and MINs were optimized directly from lowest points along AFIR paths. The parameter T_R in eq. (6) was set to 10000 K to explore a wide area of the PES. Very large γ = 1238.9 kJ/mol (T = 3000 K, 10 days) was adopted assuming high energy processes such as laser abrasion. The search was done at the SCC-DFTB[109,110] (DFTBA in G09) level using the without-Hessian algorithm.

Formation of fullerene and related carbon materials has been studied extensively

either by stochastic approaches or MD simulations.[111-115] The purpose of application of SC-AFIR here is just to show its performance in structure searches. The search was started from a random structure of C_{60} cluster, and terminated when Buckminsterfullerene was found. Since the search is stochastic and results depend on random numbers, 10 independent calculations were performed starting from 10 different initial structures. The results are summarized in Fig. 7. In this figure, the initial random structure, the first local minimum obtained by optimization of the random structure, and the final structure are shown for each independent calculation. In addition, the numbers of gradient calculations n_g required are presented. In all the calculations, Buckminsterfullerene was found within 500000 gradient calculations. The average number of gradient calculations required was 288503. Before identifying Buckminsterfullerene, a number of higher local minima were visited. On average, 1300 independent MINs were obtained during the searches. This result demonstrates that SC-AFIR can be used in prediction of unknown structures.

3.5 Fluorescence of small PAHs

Final example is automated exploration of MECI structures. MECIs of naphthalene between its singlet first excited electronic state (S_1) and singlet ground electronic state

(S_0) were searched starting from its Franck-Condon (FC) geometry. In photoreactions, molecules can have excess energy depending on absorbed photon energy. The γ should be decided depending on available excess energy. In this study, performance was examined with two different values, γ = 100.0 and 200.0 kJ/mol. The searches were done using the spin-flip TDDFT[116-118] with the BHHLYP functional and 6-31G* basis set. The without-Hessian algorithm was adopted in the SMF/SC-AFIR part, and all obtained approximate MECI structures were optimized by the GP[95]/BPU[96] method.

Fig. 8 shows all obtained MECI structures. These MECIs are consistent with those obtained for benzene.[119,120] In total, 7531 and 8708 gradient calculations were made in the searches with γ = 100.0 and 200.0 kJ/mol, respectively. Electronic energy values relative to the S_0 energy at the FC point are shown in structural labels. The S_1/S_0 energy gaps at all these MECIs were smaller than 0.1 kJ/mol, and only single value is shown. Structures obtained by the searches with γ = 100.0 and 200.0 kJ/mol are indicated by a and b, respectively. In both of the two searches, all the lowest-lying MECIs, MECI1-5, were found. The sixth lowest MECI was found only in the search with γ = 200.0 kJ/mol. This would be because there was a high barrier for H-atom transfer from the FC point to MECI6. MECI7 was relatively low in energy, but was not found in the search with γ = 100.0 kJ/mol. This happens in the SC-AFIR search starting only from the FC point.[73]

SC-AFIR starting from the FC point can find only one of similar MECIs when there are some MECIs in a similar direction. MECI7 has a deformation in the CH moiety in the right-hand side of the molecule. MECI4 also has a deformation in the same CH part. When γ is small, the lower energy ones among similar MECIs tend to be found, and for qualitative discussions the present treatment is enough. On the other hand, one can find all such MECIs when SMF/SC-AFIR is applied not only to the FC point but also to all obtained MECIs having bond connectivity of the FC structure. The other cases in which either a or b is missing can also be explained with these two reasons.

In this calculation, the lowest MECI, i.e., MECI2, in the FC region was identified. Similarly, the lowest MECIs for benzene, phenanthrene, anthracene, and pyrene in their FC regions were identified.[74] We focused on the difference between the energy at the lowest MECI and the S_1 energy at the FC point i.e., $E_{\text{Lowest-MECI}} - E_{\text{FC}}$. Then, a correlation between this energy difference and the experimental fluorescence quantum yields[121] is shown in Fig. 9.[74] The two quantities showed a nice correlation in Fig. 9. The gap $E_{\text{Lowest-MECI}} - E_{\text{FC}}$ should have a correlation with the rate of non-radiative decay. When the energy difference is large and the non-radiative decay is slow, the fluorescence quantum yield becomes large. We emphasize that such a discussion can be made only when the lowest MECI is identified. The present approach can be a powerful

tool to identify the lowest MECI in the FC region. Further investigation incorporating the contribution of triplet states is currently under progress.

4. Concluding remarks

In this study, the AFIR method has been developed as an automated reaction path search method. This method applies an artificial force between two or more fragments to push them together or to pull them apart. This can be done by adding an artificial force term to the PES. The artificial force term is given as a weighted sum of linear functions of atom-atom distances. Such a model function consisting of the PES and the artificial force term is called AFIR function. By minimizing the AFIR function starting from a given structure, the other structure that undergoes bond reorganizations between the fragments is obtained. The path obtained by minimization of the AFIR function is called AFIR path, and the AFIR path can be regarded as an *approximate* path of chemical reactions. TSs along the reaction path can be obtained by relaxing the AFIR path and optimizing maximum energy points along the path. Finally, IRC path calculations are done starting from all obtained TSs.

Reaction paths in bimolecular and multicomponent reaction can be searched systematically by the MC-AFIR algorithm, while, those for unimolecular isomerization

and dissociation can be explored by the SC-AFIR algorithm. As a demonstration, MC-AFIR was applied to Aldol reaction between formaldehyde and vinyl-alcohol. The performance of SC-AFIR was described by its application to Claisen rearrangement reaction. Furthermore, MC- and SC-AFIR were combined in a study of the full catalytic cycle of Co-catalyzed hydroformylation. In addition, a fullerene structure search in C_{60} and a conical intersection search between two lowest single electronic states of naphthalene by SC-AFIR were also presented. These numerical examples demonstrated applicability of the AFIR method to a variety of chemical problems. All these calculations were done by the latest developmental version of the GRRM program, and all functions discussed above will be available in the next update of the distribution version.

AFIR can move a geometry from one MIN to the other straightforwardly just by minimizing a single smooth function. This allows for highly efficient escaping from the initial MIN and reaching the product region. This feature is lacking in many approaches. For example, in MD based approaches, unwanted fluctuation and vibration are generally involved. Such motions are important in discussing non-equilibrium processes and in evaluation of free-energy barriers, but are nothing more than a factor to increase the cost in static path calculations. The efficient MIN-to-MIN move by AFIR enabled extensive

applications of it to various systems.

AFIR assumes that the gradient of PES at given geometries can be obtained with a reasonable accuracy. By grace of advances in quantum mechanical (QM) calculation methods, this assumption is applicable to at least low energy geometries in many reaction systems. When the collision energy parameter γ is set to a small value such as γ < 200 kJ/mol, AFIR will never visit high energy regions as shown in this paper. AFIR therefore is suited particularly to applications to PESs of QM calculations. However, in applications to electronic excited states or to highly correlated systems such as metal clusters, one must take great care in the choice of QM calculation methods.

Applications have already been made to a variety of organo and organometallic catalysis.[52-64] Catalysis of metal clusters has also been a target of previous applications.[70,71] Recent extensions allowed for studies of photoreactions.[73,74] This enabled discussions of fluorescence in relatively large molecules and non-radiative decay mechanisms in organic molecules and organometallic complexes. A kinetic analysis which can be applied to a complex reaction path network obtained by the AFIR search has also been established recently.[100] Further developments are under progress to improve efficiency of the AFIR method and also to expand its applicability. In designing new reactions, the ability of AFIR to find unexpected pathways would be a great help. It

is therefore expected that AFIR will be one of useful tools in future catalysis research.

Acknowledgements

This work is supported by a grant from Japan Science and Technology Agency with a Core Research for Evolutional Science and Technology (CREST) in the Area of "Establishment of Molecular Technology towards the Creation of New Functions" at Hokkaido University.

References

1. F. Jensen, Introduction to Computational Chemistry, 2nd ed.; Wiley, Chichester, U.K., 2007.
2. N. Koga, K. Morokuma, *Chem. Rev.* **1991**, *91*, 823-842.
3. S. Niu, M. B. Hall, *Chem. Rev.* **2000**, *100*, 353-406.
4. P. E. M. Siegbahn, M. R. A. Blomberg, *Chem. Rev.* **2000**, *100*, 421-438.
5. M. Torrent, M. Solà, G. Frenking, *Chem. Rev.* **2000**, *100*, 439-494.
6. T. Ziegler, J. Autschbach, *Chem. Rev.* **2005**, *105*, 2695-2722.
7. K. N. Houk, P. H.-Y. Cheong, *Nature* **2008**, *455*, 309-313.
8. H. B. Schlegel, *WIREs Comput. Mol. Sci.* **2011**, *1*, 790-809.

9. D. R. Yarkony, *Rev. Mod. Phys.* **1996**, *68*, 985-1013.

10. F. Bernardi, M. Olivucci, M. A. Robb, *Chem. Soc. Rev.* **1996**, *25*, 321-328.

11. A. L. Sobolewski, W. Domcke, C. Dedonder-Lardeux, C. Jouvet, *Phys. Chem. Chem. Phys.* **2002**, *4*, 1093-1100.

12. B. G. Levine, T. J. Martinez, *Annu. Rev. Phys. Chem.* **2007**, *58*, 613-634.

13. S. Maeda, T. Taketsugu, K. Ohno, K. Morokuma, *J. Am. Chem. Soc.* **2015**, *137*, 3433-3445.

14. H. B. Schlegel, *J. Comput. Chem.* **2003**, *24*, 1514-1527.

15. D. J. Wales, *Int. Rev. Phys. Chem.* **2006**, *25*, 237-282.

16. S. Maeda, Y. Harabuchi, Y. Ono, T. Taketsugu, K. Morokuma, *Int. J. Quant. Chem.* **2015**, *115*, 258-269.

17. H. L. Davis, D. J. Wales, R. S. Berry, *J. Chem. Phys.* **1990**, *92*, 4308-4319.

18. J.-Q. Sun, K. Ruedenberg, *J. Chem. Phys.* **1993**, *98*, 9707-9714.

19. C. J. Tsai, K. D. Jordan, *J. Phys. Chem.* **1993**, *97*, 11227-11237.

20. Y. Abashkin, N. Russo, *J. Chem. Phys.* **1994**, *100*, 4477-4483.

21. K. Bondensgård, F. Jensen, *J. Chem. Phys.* **1996**, *104*, 8025-8031.

22. J. P. K. Doye, D. J. Wales, *Z. Phys. D* **1997**, *40*, 194-197.

23. W. Quapp, M. Hirsch, O. Imig, D. Heidrich, *J. Comput. Chem.* **1998**, *19*,

1087-1100.

24. M. Černohorský, S. Kettou, J. Koča, *J. Chem. Inf. Comput. Sci.* **1999**, *39*, 705-712.

25. K. M. Westerberg, C. A. Floudas, *J. Chem. Phys.* **1999**, *110*, 9259-9295.

26. D. J. Wales, J. P. K. Doye, M. A. Miller, P. N. Mortenson, T. R. Walsh, *Adv. Chem. Phys.* **2000**, *115*, 1-111.

27. K. K. Irikura, R. D. Johnson, III, *J. Phys. Chem. A* **2000**, *104*, 2191-2194.

28. E. M. Müller, A. de Meijere, H. Grubmüller, *J. Chem. Phys.* **2002**, *116*, 897-905.

29. M. Dallos, H. Lischka, E. V. D. Monte, M. Hirsch, W. Quapp, *J. Comput. Chem.* **2002**, *23*, 576-583.

30. K. Ohno, S. Maeda, *Chem. Phys. Lett.* **2004**, *384*, 277-282.

31. S. Maeda, K. Ohno, *J. Phys. Chem. A* **2005**, *109*, 5742-5753.

32. K. Ohno, S. Maeda, *J. Phys. Chem. A* **2006**, *110*, 8933-8941.

33. K. Ohno, S. Maeda, *Phys. Scr.* **2008**, *78*, 058122/1-8.

34. S. Maeda, K. Ohno, K. Morokuma, *J. Phys. Chem. A* **2009**, *113*, 1704-1710.

35. J. Baker, K. Wolinski, *J. Comput. Chem.* **2011**, *32*, 43-53.

36. S. Maeda, K. Ohno, K. Morokuma, *Adv. Phys. Chem.* **2012**, *2012*, 268124/1-13.

37. P. M. Zimmerman, *J. Comput. Chem.* **2013**, *34*, 1385-1392.

38. D. Rappoport, C. J. Galvin, D. Yu. Zubarev, Alán Aspuru-Guzik, *J. Chem. Theory Comput.* **2014**, *10*, 897-907.

39. B. Schaefer, S. Mohr, M. Amsler, S. Goedecker, *J. Chem. Phys.* **2014**, *140*, 214102/1-13.

40. S. Maeda, T. Taketsugu, K. Morokuma, K. Ohno, *Bull. Chem. Soc. Jpn.* **2014**, *87*, 1315-1334.

41. E. Martínez-Núñez, *J. Comput. Chem.* **2015**, *36*, 222-234.

42. P. M. Zimmerman, *J. Comput. Chem.* **2015**, *36*, 601-611.

43. M. Bergeler, G. N. Simm, J. Proppe, M. Reiher, *J. Chem. Theory Comput.* **2015**, *11*, 5712-5722.

44. X.-J. Zhang, Z.-P. Liu, *Phys. Chem. Chem. Phys.* **2015**, *17*, 2757-2769.

45. L.-P. Wang, R. T. McGibbon, V. S. Pande, T. J. Martinez, *J. Chem. Theory Comput.* **2016**, *12*, 638-649

46. S. Maeda, K. Morokuma, *J. Chem. Phys.* **2010**, *132*, 241102/1-4.

47. S. Maeda, K. Morokuma, *J. Chem. Theory Comput.* **2011**, *7*, 2335-2345.

48. S. Maeda, K. Ohno, K. Morokuma, *Phys. Chem. Chem. Phys.* **2013**, *15*, 3683-3701.

49. S. Maeda, T. Taketsugu, K. Morokuma, *J. Comput. Chem.* **2014**, *35*, 166-173.

50. S. Maeda, Y. Harabuchi, Y. Sumiya, M. Takagi, M. Hatanaka, Y. Osada, T. Taketsugu, K. Morokuma, K. Ohno, GRRM, a developmental version at Hokkaido University.

51. S. Maeda, Y. Harabuchi, Y. Osada, T. Taketsugu, K. Morokuma, K. Ohno, GRRM14, see http://grrm.chem.tohoku.ac.jp/GRRM/index_e.html (accessed date: March 3, 2016).

52. S. Maeda, S. Komagawa, M. Uchiyama, K. Morokuma, *Angew. Chem. Int. Ed.* **2011**, *50*, 644-649.

53. S. Maeda, K. Morokuma, *J. Chem. Theory Comput.* **2012**, *8*, 380-385.

54. M. Hatanaka, S. Maeda, K. Morokuma, *J. Chem. Theory Comput.* **2013**, *9*, 2882-2886.

55. M. Hatanaka, K. Morokuma, *J. Am. Chem. Soc.* **2013**, *135*, 13972-13979.

56. R. Uematsu, S. Maeda, T. Taketsugu, *Chem. Asian J.* **2014**, *9*, 305-312.

57. G. Zeng, S. Maeda, T. Taketsugu, S. Sakaki, *Angew. Chem. Int. Ed.* **2014**, *126*, 4721-4725.

58. G. P. Petrova, H.-B. Li, K. Maruoka, K. Morokuma, *J. Phys. Chem. B* **2014**, *118*, 5154-5167.

59. R. Uematsu, E. Yamamoto, S. Maeda, H. Ito, T. Taketsugu, *J. Am. Chem. Soc.*

2015, 137, 4090-4099.

60. S. A. Moteki, H. Maruyama, K. Nakayama, H.-B. Li, G. Petrova, S. Maeda, K. Morokuma, K. Maruoka, *Chem. Asian J.* **2015**, *10*, 2112-2116.

61. M. Hatanaka, K. Morokuma, *ACS Catal.* **2015**, *5*, 3731-3739.

62. R. Ramozzi, K. Morokuma, *J. Org. Chem.* **2015**, *80*, 5652-5657.

63. M. Puripat, R. Ramozzi, M. Hatanaka, W. Parasuk, V. Parasuk, K. Morokuma, *J. Org. Chem.* **2015**, *80*, 6959-6967.

64. W. M. C. Sameera, M. Hatanaka, T. Kitanosono, S. Kobayashi, K. Morokuma, *J. Am. Chem. Soc.* **2015**, *137*, 11085-11094.

65. S. Maeda, R. Saito, K. Morokuma, *J. Phys. Chem. Lett.* **2011**, *2*, 852-857.

66. Y. Matsuda, K. Hoki, S. Maeda, K.-i. Hanaue, K. Ohta, K. Morokuma, N. Mikami, A. Fujii, *Phys. Chem. Chem. Phys.* **2012**, *14*, 712-719.

67. P. Farahani, S. Maeda, J. S. Francisco, M. Lundberg, *ChemPhysChem* **2015**, *16*, 181-190.

68. S. Maeda, E. Abe, M. Hatanaka, T. Taketsugu, K. Morokuma, *J. Chem. Theory Comput.* **2012**, *8*, 5058-5063.

69. M. Isegawa, S. Maeda, D. J. Tantillo, K. Morokuma, *Chem. Sci.* **2014**, *5*, 1555-1560.

70. M. Gao, A. Lyalin, S. Maeda, T. Taketsugu, *J. Chem. Theory Comput.* **2014**, *10*, 1623-1630.

71. M. Gao, A. Lyalin, M. Takagi, S. Maeda, T. Taketsugu, *J. Phys. Chem. C* **2015**, *119*, 11120-11130.

72. S. Maeda, T. Taketsugu, K. Morokuma, *Z. Phys. Chem.* **2013**, *227*, 1421-1433.

73. S. Maeda, Y. Harabuchi, T. Taketsugu, K. Morokuma, *J. Phys. Chem. A* **2014**, 118, 12050-12058.

74. Y. Harabuchi, T. Taketsugu, S. Maeda, *Phys. Chem. Chem. Phys.* **2015**, *17*, 22561-22565.

75. D. Murdock, R. A. Ingle, I. V. Sazanovich, I. P. Clark, Y. Harabuchi, T. Taketsugu, S. Maeda, A. J. Orr-Ewing, M. N. R. Ashfold, *Phys. Chem. Chem. Phys.* **2015**, *18*, 2629-2638.

76. A. Fernández-Ramos, J. A. Miller, S. J. Klippenstein, D. G. Truhlar, *Chem. Rev.* **2006**, *106*, 4518-4584.

77. J. C. Phillips, R. Braun, W. Wang, J. Gumbart, E. Tajkhorshid, E. Villa, C. Chipot, R. D. Skeel, L. Kalé, K. Schulten, *J. Comput. Chem.* **2005**, *26*, 1781-1802.

78. M. T. Ong, J. Leiding, H. Tao, A. M. Virshup, T. J. Martinez, *J. Am. Chem. Soc.*

2009, *131*, 6377-6379.

79. J. Ribas-Arino, M. Shiga, D. Marx, *Angew. Chem. Int. Ed.* **2009**, *48*, 4190-4193.

80. K. Wolinski, J. Baker, *Mol. Phys.* **2009**, *107*, 2403-2417.

81. G. Fogarasi, X. Zhou, P. W. Taylor, P. Pulay, *J. Am. Chem. Soc.* **1992**, *114*, 8191-8201.

82. K. Fukui, *J. Phys. Chem.* **1970**, *74*, 4161-4163.

83. K. Fukui, *Acc. Chem. Res.* **1981**, *14*, 363-368.

84. R. Elber, M. Karplus, *Chem. Phys. Lett.* **1987**, *139*, 375-380.

85. C. Choi, R. Elber, *J. Chem. Phys.* **1991**, *94*, 751-760.

86. P. Y. Ayala, H. B. Schlegel, *J. Chem. Phys.* **1997**, *107*, 375-384.

87. G. Henkelman, B. P. Uberuaga, H. Jónsson, *J. Chem. Phys.* **2000**, *113*, 9901-9904.

88. W. E, W. Ren, E. Vanden-Eijnden, *Phys. Rev. B* **2002**, *66*, 052301/1-4.

89. B. Peters, A. Heyden, A. T. Bell, A. Chakraborty, *J. Chem. Phys.* **2004**, *120*, 7877-7886.

90. A. Banerjee, N. Adams, J. Simons, R. Shepard, *J. Phys. Chem.* **1985**, *89*, 52-57.

91. P. Culot, G. Dive, V. H. Nguyen, J. M. Ghuysen, *Theor. Chim. Acta* **1992**, *82*, 189-205.

92. J. M. Bofill, *J. Comput. Chem.* **1994**, *15*, 1-11.

93. Ö. Farkas, H. B. Schlegel, *J. Chem. Phys.* **1999**, *111*, 10806-10814.

94. M. Page, J. W. McIver, Jr., *J. Chem. Phys.* **1988**, *88*, 922-935.

95. M. J. Bearpark, M. A. Robb, H. B. Schlegel, *Chem. Phys. Lett.* **1994**, *223*, 269-274.

96. S. Maeda, K. Ohno, K. Morokuma, *J. Chem. Theory Comput.* **2010**, *6*, 1538-1545.

97. L. Kürti, B. Czakó, Strategic Applications of Named Reactions in Organic Synthesis; Elsevier B.V.: Amsterdam, **2005**.

98. F. W. Schuler, W. M. George, *J. Am. Chem. Soc.* **1950**, *72*, 3155-3159.

99. R. L. Vance, N. G. Rondan, K. N. Houk, F. Jensen, W. Thatcher Borden, A. Komornicki, E. Wimmer, *J. Am. Chem. Soc.* **1988**, *110*, 2314-2315.

100. Y. Sumiya, Y. Nagahata, T. Komatsuzaki, T. Taketsugu, S. Maeda, *J. Phys. Chem. A* **2015**, *119*, 11641-11649.

101. Y. Nagahata, S. Maeda, H. Teramoto, T. Horiyama, T. Taketsugu, and T. Komatsuzaki, *J. Phys. Chem. B* **2016**, *120*, 1961-1971.

102. F. Hebrard, P. Kalck, *Chem. Rev.* **2009**, *109*, 4272-4282.

103. R. F. Heck, D. S. Breslow, *J. Am. Chem. Soc.* **1961**, *83*, 4023-4027.

104. L. Versluis, T. Ziegler, E. J. Baerends, W. Ravenek, *J. Am. Chem. Soc.* **1989**, *111*, 2018-2025.

105. L. Versluis, T. Ziegler, L. Fan, *Inorg. Chem.* **1990**, *29*, 4530-4536.

106. C.-F. Huo, Y.-W. Li, M. Beller, H. Jiao, *Organometallics* **2003**, *22*, 4665-4677.

107. C.-F. Huo, Y.-W. Li, M. Beller, H. Jiao, *Organometallics* **2005**, *24*, 3634-3643.

108. L. E. Rush, P. G. Pringle, J. N. Harvey, *Angew. Chem., Int. Ed.* **2014**, *53*, 8672-8676.

109. M. Elstner, D. Porezag, G. Jungnickel, J. Elsner, M. Haugk, T. Frauenheim, S. Suhai, G. Seifert, *Phys. Rev. B* **1998**, *58*, 7260-7268.

110. G. Zheng, H. Witek, P. Bobadova-Parvanova, S. Irle, D. G. Musaev, R. Prabhakar, K. Morokuma, M. Lundberg, M. Elstner, C. Kohler, T. Frauenheim, *J. Chem. Theory Comput.* **2007**, *3*, 1349-1367.

111. D. M. Deaven, K. M. Ho, *Phys. Rev. Lett.* **1995**, *75*, 288-291.

112. D. J. Wales, M. A. Miller, T. R. Walsh, *Nature* **1999**, *394*, 758-760.

113. S, Irle, G. Zheng, Z. Wang, K. Morokuma, *J. Phys. Chem. B* **2006**, *110*, 14531-14545.

114. X.-J. Zhang, C. Shang, Z.-P. Liu, *J. Chem. Theory Comput.* **2013**, *9*, 3252-3260.

115. A. J. Page, F. Ding, S. Irle, K. Morokuma, *Rep. Prog. Phys.* **2015**, *78*, 036501.

116. Y. H. Shao, M. Head-Gordon, A. I. Krylov, *J. Chem. Phys.* **2003**, *118*, 4807-4818.

117. F. Wang, T. Ziegler, *J. Chem. Phys.* **2004**, *121*, 12191-12196.

118. N. Minezawa, M. S. Gordon, *J. Phys. Chem. A* **2009**, *113*, 12749-12753.

119. Q. Li, D. Mendive-Tapia, M. J. Paterson, A. Migani, M. J. Bearpark, M. A. Robb, L. Blancafort, *Chem. Phys.* **2010**, *377*, 60-65.

120. L. Blancafort, M. A. Robb, *J. Chem. Theory Comput.* **2012**, *8*, 4922-4930.

121. The Chemical Society of Japan, Kagaku Binran (Kisohen 1) 5th ed., Maruzen, Tokyo, **2004**.

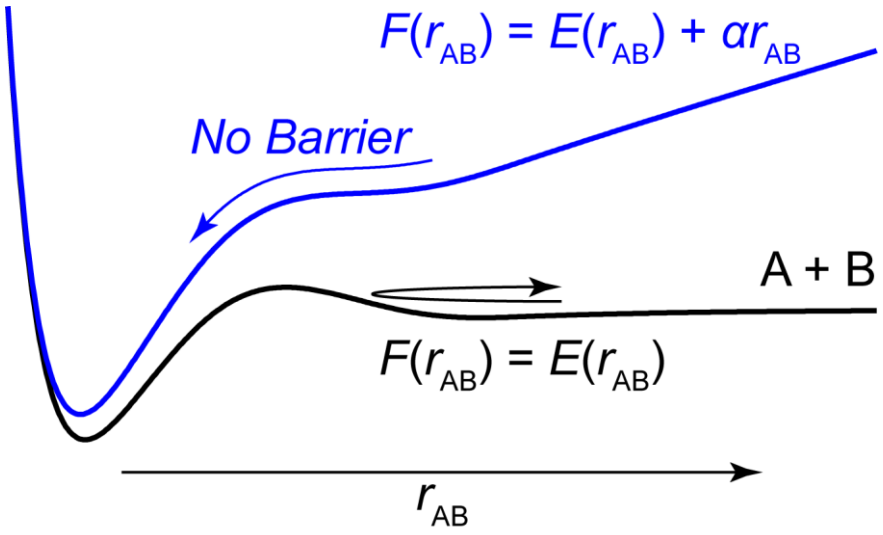

Fig. 1. A diatomic potential curve $E(r_{AB})$ between atoms A and B (see the black curve) and the corresponding AFIR function $E(r_{AB}) + \alpha r_{AB}$ (see the blue curve). r_{AB} is the distance between A and B, and α is a constant parameter.

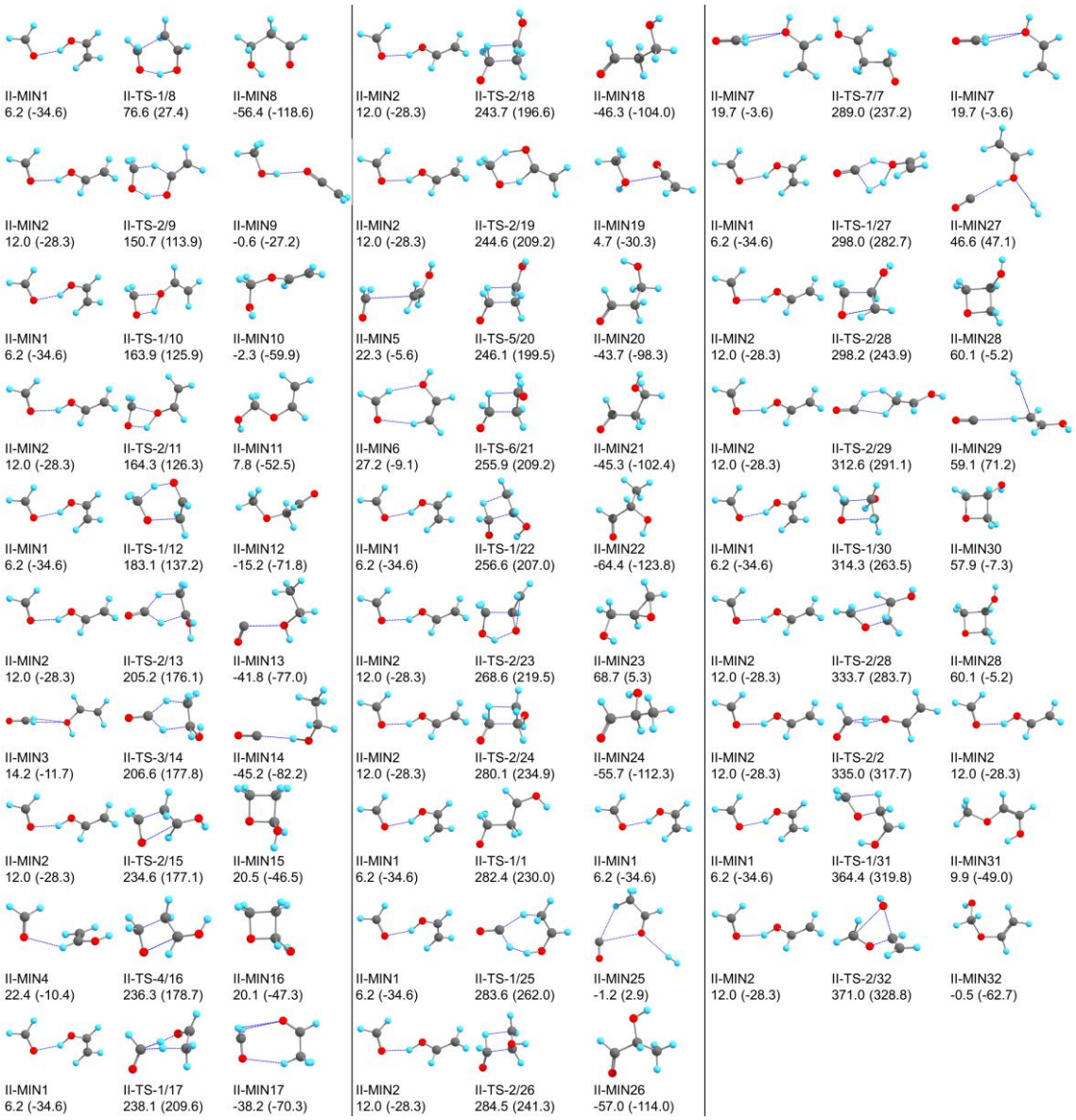

Fig. 2. Bond reorganization pathways obtained by MC-AFIR for the bimolecular reaction between formaldehyde and vinyl alcohol. TS*x*/*y* is a transition state connecting MIN*x* and MIN*y* in this figure. Gibbs free energy and electronic energy in parentheses relative to separately optimized reactants are shown in kJ/mol.

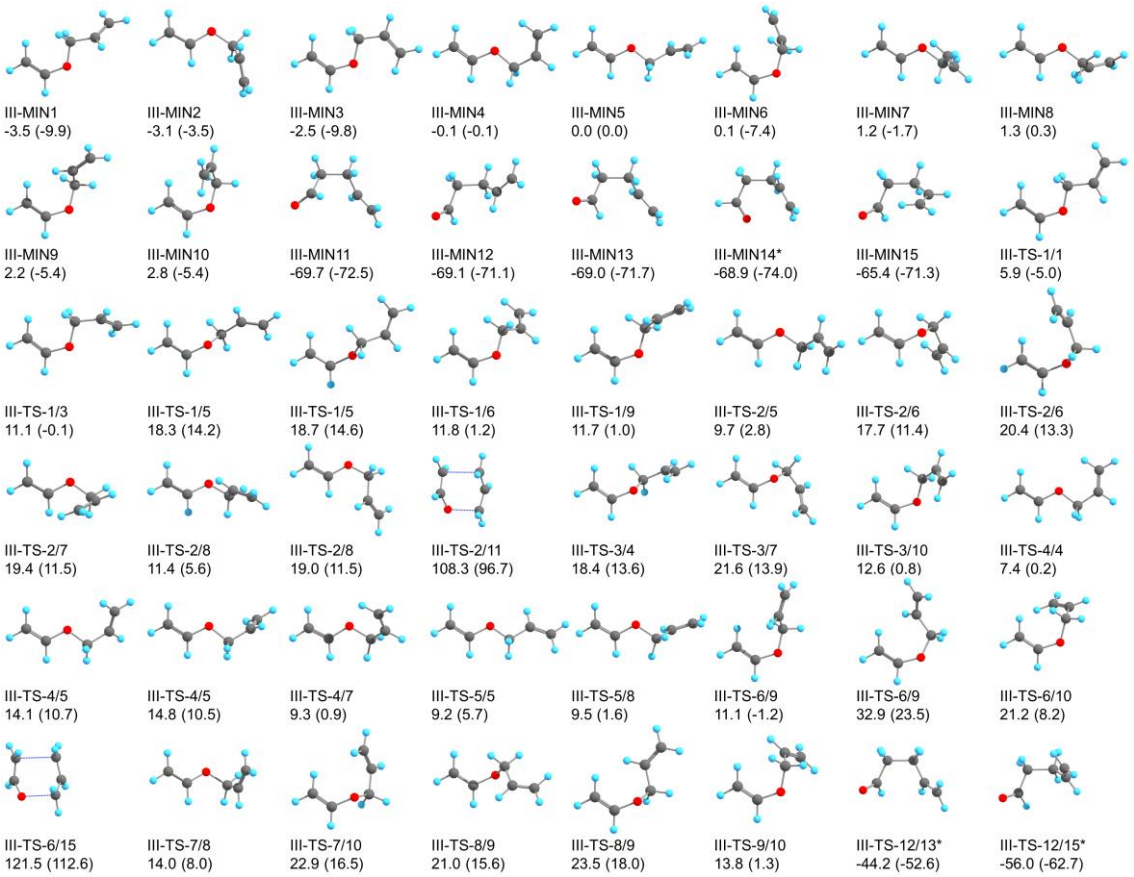

Fig. 3. Reaction pathways obtained by SC-AFIR for the unimolecular reaction of allyl vinyl ether. TS*x*/*y* is a transition state connecting MIN*x* and MIN*y* in this figure. Gibbs free energy and electronic energy in parentheses relative to separately optimized reactants are shown in kJ/mol. Structures missed by the without-Hessian algorithm are indicated by *.

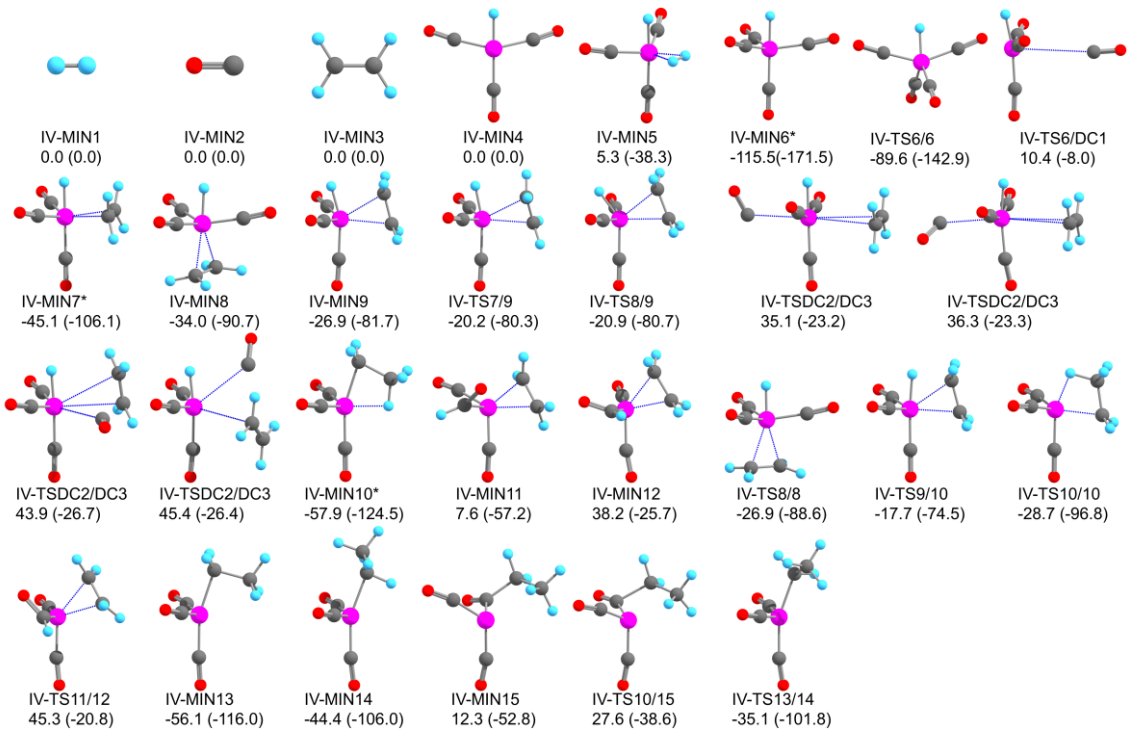

Fig. 4. Reaction pathways obtained by MC- and SC-AFIR for the initial part of Co-catalyzed hydroformylation. TS*x*/*y* is a transition state connecting MIN*x* and MIN*y* in this figure. Gibbs free energy and electronic energy in parentheses relative to separately optimized reactants are shown in kJ/mol. DC stands for dissociation channel: DC1 is $HCo(CO)_3$ + CO at 0.0 (0.0) kJ/mol, DC2 is MIN7 + CO at −45.1 (−106.1) kJ/mol, and DC3 is MIN6 + C_2H_4 at −115.5 (−171.5) kJ/mol.

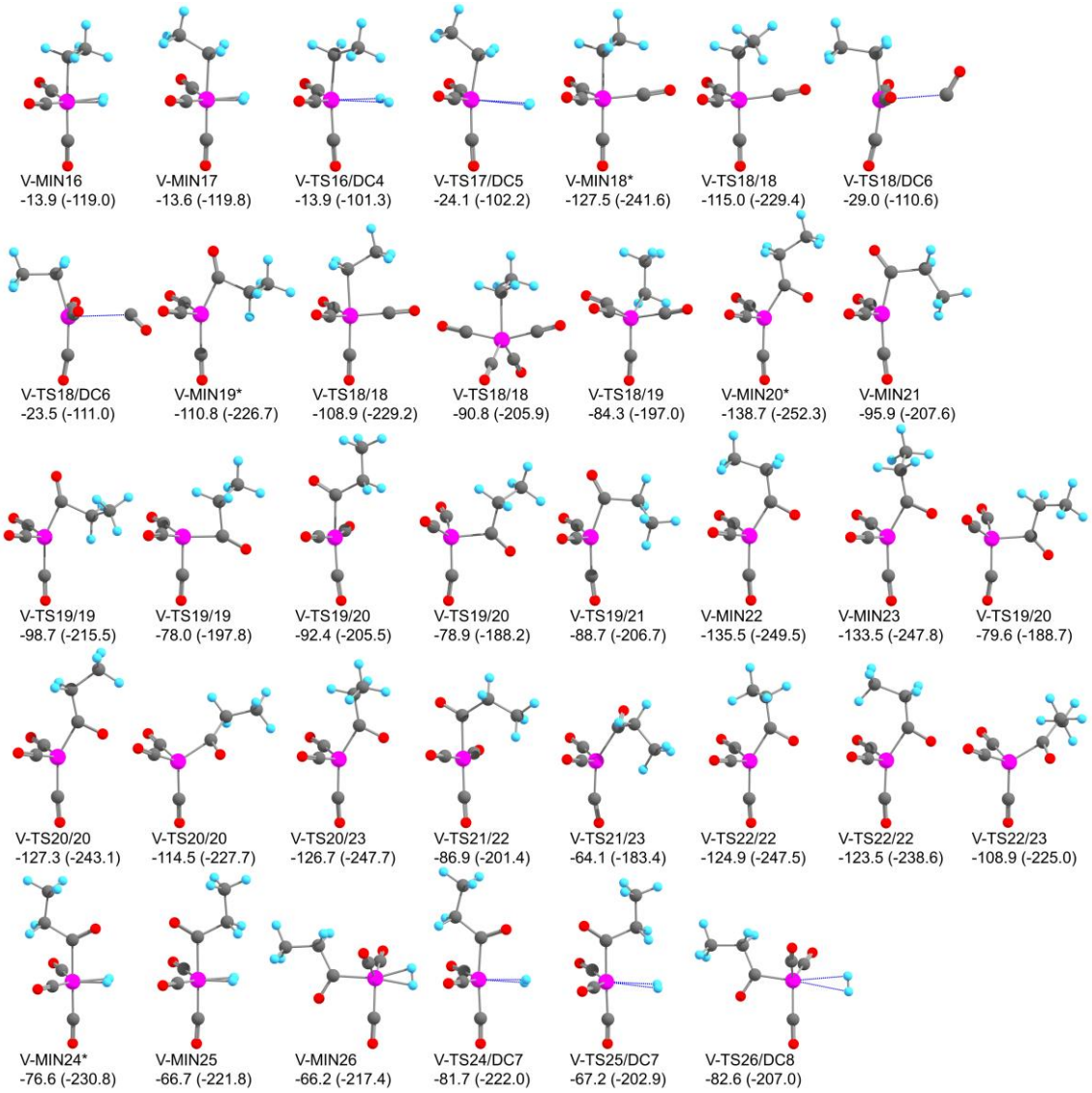

Fig. 5. Reaction pathways obtained by MC- and SC-AFIR for the middle part of Co-catalyzed hydroformylation. TS*x*/*y* is a transition state connecting MIN*x* and MIN*y* in this figure or in Fig. 4. Gibbs free energy and electronic energy in parentheses relative to separately optimized reactants are shown in kJ/mol. DC stands for dissociation channel: DC4 is MIN13 + H_2 at −56.1 (−116.0) kJ/mol, DC5 is MIN14 + H_2 at −44.4 (−106.0) kJ/mol, DC6 is MIN13 + CO at −56.1 (−116.0) kJ/mol, DC7 is

MIN20 + H_2 at −138.7 (−252.3) kJ/mol, and DC8 is MIN19 + H_2 at −110.8 (−226.7) kJ/mol.

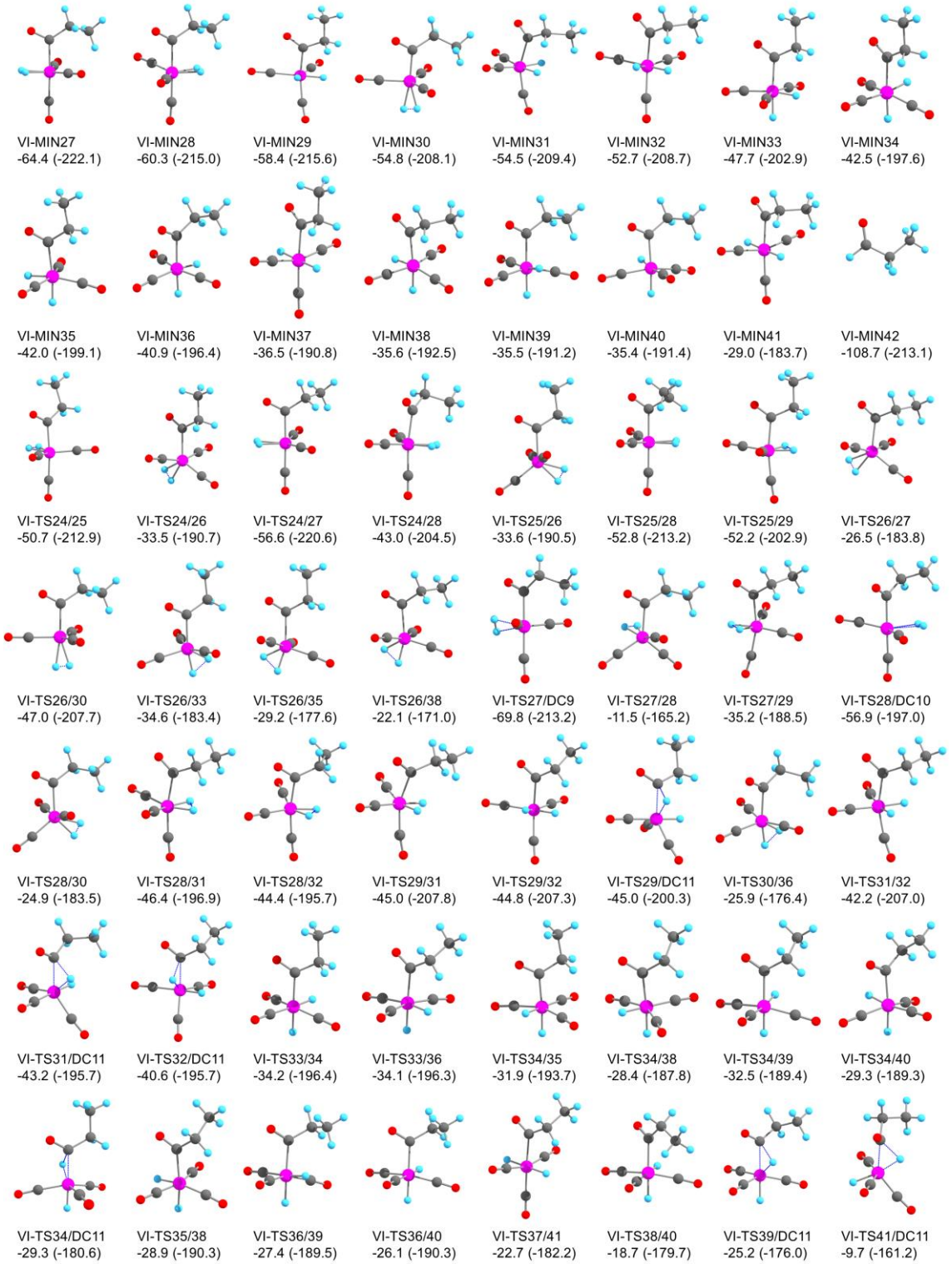

Fig. 6. Reaction pathways obtained by MC- and SC-AFIR for the last part of Co-catalyzed hydroformylation. TS*x*/*y* is a transition state connecting MIN*x* and MIN*y*

in this figure, in Fig. 4, or in Fig. 5. Gibbs free energy and electronic energy in parentheses relative to separately optimized reactants are shown in kJ/mol. DC stands for dissociation channel: DC9 is MIN22 + H_2 at −135.5 (−249.5) kJ/mol, DC10 is MIN19 + H_2 at −110.8 (−226.7) kJ/mol, DC11 is MIN42 + $HCo(CO)_3$ at −108.7 (−213.1) kJ/mol.

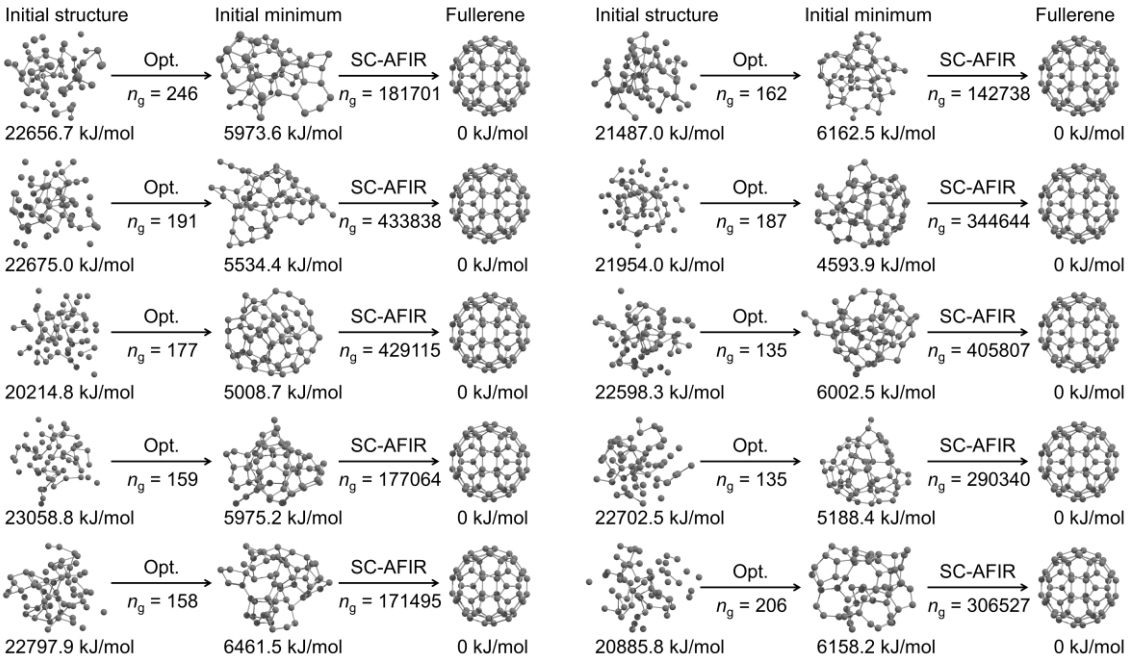

Fig. 7. Initial random structure, initial local minimum structure obtained by optimization of the random structure, and the final structure seen in the 10 independent stochastic SC-AFIR searches. The number of gradients computed in each step n_g is shown below arrows. Electronic energy relative to Buckminsterfullerene is shown below each structure.

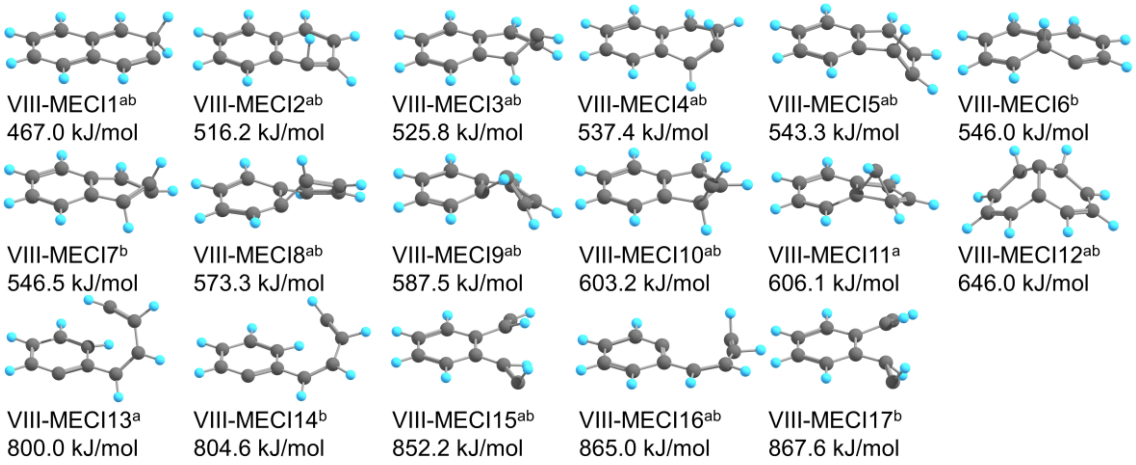

Fig. 8. Minimum energy conical intersection (MECI) structures of naphthalene between its singlet first excited electronic state (S_1) and the singlet ground electronic state (S_0), obtained by the SMF/SC-AFIR search starting from the Franck-Condon (FC) geometry. Electronic energy relative to the S_0 energy of the FC point are shown. The energy gap between the two target states are smaller than 0.1 kJ/mol, and only single value is shown. Structures obtained by the searches with γ = 100 and 200 kJ/mol, respectively, are indicated by a and b.

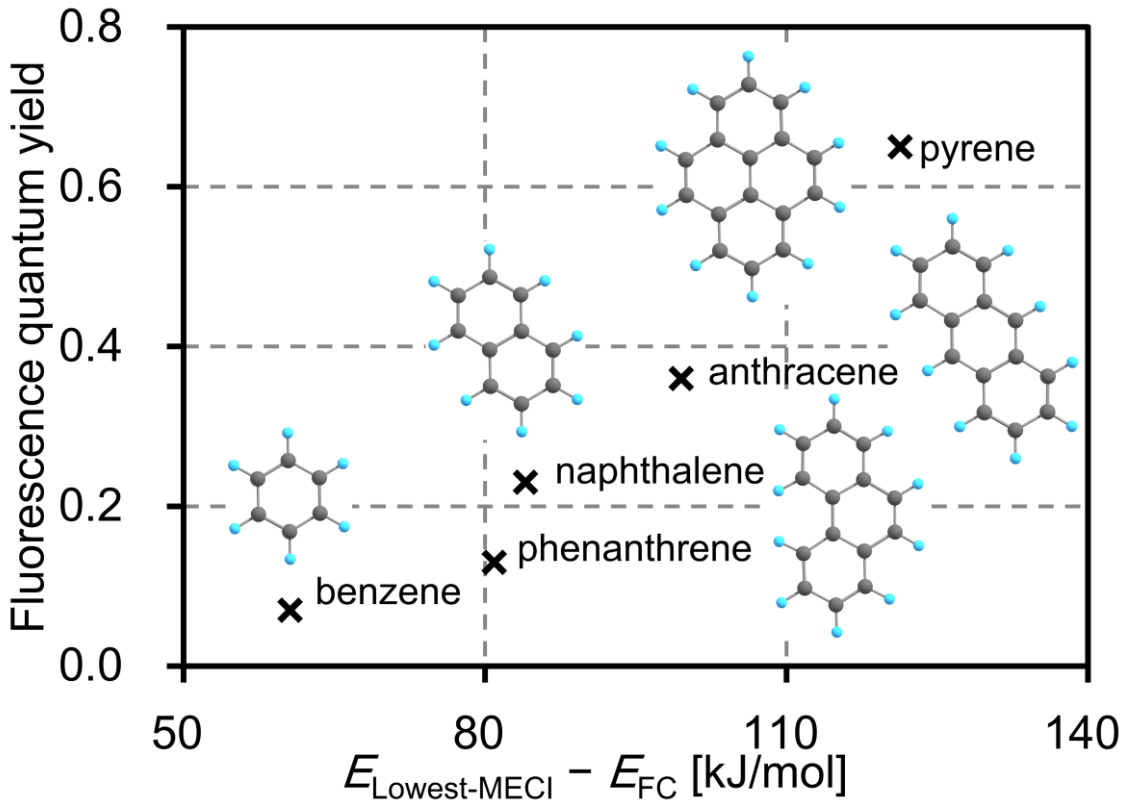

Fig. 9. The correlation between the fluorescence quantum yields measured in cyclohexane,[121] and the energy difference, $E_{\text{Lowest-MECI}} - E_{\text{FC}}$ (cross marks). Each PAH is indicated with the structure and name of the PAH. Reproduced from Ref. 74 with permission from the Royal Society of Chemistry.

Biography

Satoshi Maeda received his Ph.D. from Tohoku University in 2007 under the guidance of Prof. Koichi Ohno. In 2007-2010, he did postdoctoral work as a JSPS research fellow at Tohoku University and Toyota Physical and Chemical Research Institute. In 2008-2010, he visited Emory University and Kyoto University and made collaborations with Prof. Keiji Morokuma. In 2010-2011, he was an Assistant Professor of the Hakubi project at Kyoto University. Since 2012, he has worked with Prof. Tetsuya Taketsugu at Hokkaido University as an Assistant Professor until 2013 and currently as an Associate Professor. He has worked on development of automated methods for systematic exploration of quantum chemical potential energy surfaces, and on applications of these methods to analysis and prediction of molecular structures and reaction mechanisms

Yu Harabuchi received his Ph.D. from Hokkaido University in 2013 under the supervision of Prof. Tetsuya Taketsugu. He was a JSPS research fellow from 2012 to 2014. In 2013, he joined Prof. Mark S. Gordon's group at Iowa State University as a postdoctoral fellow. In 2014, he returned to Hokkaido University as a postdoctoral fellow and worked with Prof. Tetsuya Taketsugu and Prof. Satoshi Maeda. His current research interests focus on theoretical investigations of photo-reactions based on dynamics simulations and automated search methods for conical intersections.

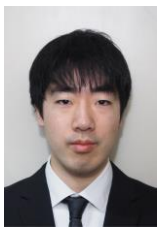

Makito Takagi received his Master’s degree from Hokkaido University in 2016. Currently, he is a Ph.D student of Hokkaido University and doing his research under the guidance of Prof. Tetsuya Taketsugu and Prof. Satoshi Maeda. His research interests focus on structure prediction of clusters and crystals.

Tetsuya Taketsugu received his Ph.D. from the University of Tokyo in 1994 under the guidance of Prof. Tsuneo Hirano, and did posdoc with Prof. Mark Gordon at Iowa State University. He worked as Assistant Professor with Prof. Kimihiko Hirao at the University of Tokyo from 1995-1999, and was Associate Professor at Ochanomizu University from 1999-2005. Since 2005, he has been Professor of Quantum Chemistry Laboratory in Hokkaido University. His research interests focus on the development of the methodology to explore potential energy surfaces and on-the-fly dynamics, as well as theoretical approach to design a novel catalyst.

Keiji Morokuma finished PhD at Kyoto University in 1963 under Prof. Kenichi Fukui and did postdoc with Prof. Martin Karplus at Harvard and Columbia University; he is proud to have two Nobel Laureates as supervisors. From 1967-1977 he moved up the ladder to Professor at University of Rochester, from 1977-1992 he was Professor at the Institute for Molecular Science, Okazaki, Japan and from 1993-2006 he was William H. Emerson Professor at Emory University. Since 2006 he has been at the Fukui Institute for Fundamental Chemistry, Kyoto University. He has worked on developments of theoretical methods, such as EDA, ONIOM, and GRRM, and on applications to many chemical problems, including catalysis.